Robotica (2026), **44**, pp. 1652–1672
doi:10.1017/S0263574726103713

CAMBRIDGE UNIVERSITY PRESS

RESEARCH ARTICLE

Lumped parameter collision modeling of robotic manipulators based on the effective mass approach

Andrea Cesaro, Michele Tonan, Matteo Bottin, Alberto Doria and Giulio Rosati

Department of Industrial Engineering, Università degli Studi di Padova, Italy
Corresponding author: Matteo Bottin; Email: matteo.bottin@unipd.it

Received: 18 June 2025 UTC; **Revised:** 19 January 2026 UTC; **Accepted:** 7 June 2026 UTC;
First published online: 13 July 2026 UTC

Keywords: robot collision; lumped parameter modeling; robotic manipulator; effective mass; safety

Abstract

The increasing adoption of robotic manipulators in the industry has brought the issue of robotic device safety to the forefront, particularly in the context of collaborative robotics. Among the main challenges, the evaluation of impacts with operators and objects in the workspace represents a critical issue, as accurately quantifying the magnitude of collisions is a complex task. Although current regulations propose various models for impact assessment, the suggested approaches are often oversimplified and not easily applicable in complex scenarios. To overcome this limitation, this study proposes the development of an effective mass impact model that simulates the collision between two bodies as an interaction between two lumped masses. The model is developed for both two-dimensional and three-dimensional analyses. Furthermore, it is implemented in a generic form and using a lumped-parameter robot model. This formulation enables the creation of a highly versatile model capable of overcoming the lack of knowledge of inertial parameters of robots. The approach is experimentally validated by means of a SCARA robot that collides with a cart, demonstrating the model's applicability and accuracy.

1. Introduction

Human–robot collaboration plays a significant role in industry since it contributes to increasing productivity and efficiency. However, this collaboration has introduced safety standards different from traditional industrial robotics [1]. They focus on the prevention of human–robot impacts and on the minimization of related risks or their consequences to achieve a safe collaborative human–robot environment. These standards have driven research efforts in collision estimation, which, as discussed in the literature, is relatively straightforward in the case of one- or two-dimensional interactions between objects of known shape and under the assumption of elastic or perfectly inelastic impacts [2]. Many contact models have been proposed in the years [3, 4]. The extension of the theory to impacts in the 3D space increases the complexity of the mathematical model. Although these issues have been addressed in the literature, accurate modeling of collisions remains a challenging task [5].

The ISO 10218-2:2025 standard [6] that includes the old ISO/TS 15066:2016 standard [7] aims to simplify the complexity of the impacts by assuming the collision is perfectly inelastic, that is, the coefficient of restitution is considered equal to zero. However, this leads to some simplifications, which yield a discrepancy between the model and the real impact phenomena. As a result, several tests have been carried out to analyze impact forces by simulating collisions between robots and operators. Rosenstrauch and Krüger [8] provided a more detailed insight into ISO/TS 15066 and carried out an experiment with a benchmark standard collaboration scenario, demonstrating its usage; Falco et al. [9] provided an overview of the currently proposed injury metrics and described a prototype measurement device that replicates the deformation constants of the various body regions and measures static and dynamic collision forces during robot collisions; Dagalakis et al. [10] described the dynamic impact testing and

© The Author(s), 2026. Published by Cambridge University Press. This is an Open Access article, distributed under the terms of the Creative Commons Attribution licence (https://creativecommons.org/licenses/by/4.0/), which permits unrestricted re-use, distribution and reproduction, provided the original article is properly cited.

https://doi.org/10.1017/S0263574726103713 Published online by Cambridge University Press

calibration instrument, a simple instrument with significant data collection and analysis capabilities that is used to measure the severity of injuries caused in the case of a robot impact with a human.

Beyond impact modeling and experimental force assessment, several studies have addressed collision mitigation at the control level. Impedance-based control strategies have been widely adopted to ensure safe human–robot interaction by shaping the dynamic behavior of the robot during contact [11]. Such approaches, however, rely on timely and reliable information about the interaction dynamics, highlighting the importance of simplified and computationally efficient models for force estimation and safety-oriented design.

To bypass the complexity of the impacts of multi-link 3D robots, simplified impact models can be developed using the effective mass concept [12]. The effective mass represents the mass perceived at the operational point, such as the end-effector, in response to the application of a force in a specific direction [13]. This approach makes it possible to describe the collision as an interaction between two lumped masses along the impact direction. The concept has been applied in several contexts: Kirschner et al. [14] proposed a method to practically determine the effective mass using a passive mechanical pendulum setup, while Kang et al. [15] proposed the combined potential function method considering both the minimum effective mass and joint limit constraints in order to find the optimized configuration through redundant motion.

This paper aims to adopt the effective mass approach and simplify the impact model using lumped parameters. The proposed approach approximates the real inertia tensor without compromising the validity or accuracy of the model [16, 17]. The simplified model can be used in place of the full model (i.e., the one without simplifications) when no exact data about the inertia tensor of the robot are available, or when the computational time is a key issue for real-time applications [17]. Impact tests using a SCARA robot against a sliding block were performed to validate the mathematical model with the effective mass approach. The impact force was used as a benchmark to compare the theoretical model and assess the validity of our method.

The main contributions of the paper are

- the extension of a general effective mass approach for modeling robot collisions;
- the formulation of a simplified lumped parameter model that does not require knowledge of the robot's inertia tensors;
- a comparative analysis of the effective and reduced mass values obtained from the full model, the simplified model, and the ISO standard model;
- the experimental validation of the proposed model using a SCARA robot impacting a cart.

The article is structured as follows: Section 2 introduces the mathematical models for effective mass computation. The full model, the simplified model, and the standard model are presented. Section 3 describes the lumped model and the effective mass calculation for a SCARA robot. Section 4 shows the comparison between the three models. Section 5 describes the experimental setup of a SCARA robot that impacts a sliding block along a linear guide and makes a comparison between theoretical and experimental results. Finally, in Section 6, conclusions are drawn.

2. Effective mass computation

In the case of controlled mechanisms (e.g., robots), the mechanism configuration depends on the controlled joint variables $\boldsymbol{q}$. The velocity of the impact point in the Cartesian space $\dot{\boldsymbol{x}}$[1] is defined by the well-known Jacobian matrix $\boldsymbol{J}(\boldsymbol{q})$:

$$\dot{\boldsymbol{x}} = \boldsymbol{J}(\boldsymbol{q})\dot{\boldsymbol{q}} \tag{1}$$

[1] Please note that velocity $\dot{\boldsymbol{x}} = [v_x\ v_y\ v_z\ \omega_x\ \omega_y\ \omega_z]^T$ contains both the linear and angular velocities of the link.

https://doi.org/10.1017/S0263574726103713 Published online by Cambridge University Press

The number, m, of independent parameters needed to describe the position and orientation of the end-effector determines the degrees of freedom. When the end-effector and the manipulator have both the same degree of freedom (i.e., $n = m$), the operational coordinates, $\boldsymbol{x}$, form a set of generalized coordinates for the mechanism [18]. In this case, the kinetic energy of the mechanism is a quadratic form of the generalized operational velocities and can be expressed as:

$$E_k = \frac{1}{2}\dot{\boldsymbol{x}}^T \boldsymbol{\Lambda}(\boldsymbol{q})\dot{\boldsymbol{x}} \tag{2}$$

where $\boldsymbol{\Lambda}(\boldsymbol{q})$ is the $n \times n$ mass matrix associated with the operational space. $\boldsymbol{\Lambda}(\boldsymbol{q})$ can be expressed as a function of $\boldsymbol{q}$, as it depends on $\boldsymbol{x}$, which is itself a function of $\boldsymbol{q}$.

The operational mass matrix $\boldsymbol{\Lambda}(\boldsymbol{q})$ provides a description of the inertial properties of the manipulator at the operational point. The relationship between the operational mass matrix $\boldsymbol{\Lambda}(\boldsymbol{q})$ and the joint-space mass matrix $\boldsymbol{M}(\boldsymbol{q})$ can be established by stating the identity between the two quadratic forms of kinetic energy and by using the relationship between joint velocities and end-effector velocities, which involves the Jacobian matrix, $\boldsymbol{J}(\boldsymbol{q})$. Matrix $\boldsymbol{\Lambda}(\boldsymbol{q})$ can be computed as follows:

$$\boldsymbol{\Lambda}(\boldsymbol{q}) = \boldsymbol{J}^{-T}(\boldsymbol{q})\boldsymbol{M}(\boldsymbol{q})\boldsymbol{J}^{-1}(\boldsymbol{q}) \tag{3}$$

Let us consider the task of positioning the end-effector. The Jacobian in this case is the matrix, $\boldsymbol{J}_v(\boldsymbol{q})$, associated with the linear velocity at the operational point. The operational mass matrix is

$$\boldsymbol{\Lambda}_v^{-1}(\boldsymbol{q}) = \boldsymbol{J}_v(\boldsymbol{q})\boldsymbol{M}^{-1}(\boldsymbol{q})\boldsymbol{J}_v^T(\boldsymbol{q}) \tag{4}$$

The velocity of the impact point can be decomposed into three components: the first two lie within the plane tangent to the surfaces of the two bodies in contact, while the third is perpendicular to this plane and lies along the common normal. The first two velocity components result in sliding between the bodies, which leads to friction forces. The third component, on the other hand, causes a penetration between the bodies, generating impact forces according to the impact models presented in the literature [4]. For this reason, in this work, only the forces exchanged during the impact along the common normal are considered.

If only the normal direction ($\boldsymbol{n}$) to the contact point is considered, the Jacobian $\boldsymbol{J}_v(\boldsymbol{q})$ has a single row:

$$\boldsymbol{J}_{vn}(\boldsymbol{q}) = \boldsymbol{n}^T\boldsymbol{J}_v(\boldsymbol{q}) \tag{5}$$

The operational mass matrix in this case is a scalar, m_n, representing the mass perceived at the end-effector in response to the application of a force along $\boldsymbol{n}$:

$$m_n = \boldsymbol{J}_{vn}^{-T}(\boldsymbol{q})\boldsymbol{M}(\boldsymbol{q})\boldsymbol{J}_{vn}^{-1}(\boldsymbol{q}) \tag{6}$$

To avoid computing the noninvertible vector $\boldsymbol{J}_{vn}^{-T}$, an inverse operation is performed on the entire expression. The result is

$$\frac{1}{m_n} = \boldsymbol{J}_{vn}(\boldsymbol{q})\boldsymbol{M}^{-1}(\boldsymbol{q})\boldsymbol{J}_{vn}^T(\boldsymbol{q}) \tag{7}$$

Substituting Eqs. (4) and (5) into (7), the expression of m_n becomes:

$$m_n = \frac{1}{\boldsymbol{n}^T\boldsymbol{\Lambda}_v^{-1}(\boldsymbol{q})\boldsymbol{n}} \tag{8}$$

This approach can be applied to any mechanism, provided that the mass matrix $\boldsymbol{M}(\boldsymbol{q})$ can be calculated and the mechanism is not in a singular configuration.

In this paper, the effective mass models will be applied to serial open-chain robots. Three theoretical impact models will be compared, namely:

- *Full model*, a model that considers the entire mechanical model of the serial robot, including both the mass and the inertia tensor of the links;

https://doi.org/10.1017/S0263574726103713 Published online by Cambridge University Press

- *Simplified model*, a model that simplifies the mechanical structure of the robot by representing the link with only lumped masses, as shown in [17];
- *Standard model*, the model that applies the ISO 10218-2:2025 standard to the collision between a robot and a human body.

The human body is replaced by a generic obstacle mass, which will be included in the experimental tests.

In the following sections, the calculation of the mass matrix $\boldsymbol{M}(\boldsymbol{q})$ is explained for the first two models, whereas for the third model, the direct computation of the effective mass is presented according to the ISO standard.

2.1. Full model

In the full model, the mass matrix of the robot is calculated by means of the Lagrangian approach. Both the kinetic energy due to the masses of the links and the kinetic energy due to the inertia tensors of the links [19] are considered. The mass matrix can be calculated as:

$$\boldsymbol{M}(\boldsymbol{q}) = \sum_{i=1}^{n} \left(m_i \boldsymbol{J}_P^{(i)T} \boldsymbol{J}_P^{(i)} + \boldsymbol{J}_O^{(i)T} \boldsymbol{R}_i \boldsymbol{I}_i \boldsymbol{R}_i^T \boldsymbol{J}_O^{(i)} \right) \tag{9}$$

where m_i and $\boldsymbol{I}_i$ represent the mass and the inertia tensor calculated at the center of mass (CoM) of the i-th link, respectively, $\boldsymbol{J}_P^{(i)}$ and $\boldsymbol{J}_O^{(i)}$ are the two Jacobians that represent the relationships between the joint velocities and the linear and angular velocities of the i-th link, respectively, n is the number of links, and $\boldsymbol{R}_i$ is the rotation matrix from the reference frame of the i-th link and the base frame.

The Jacobians are

$$\boldsymbol{J}_P^{(l,i)} = \begin{bmatrix} \boldsymbol{j}_{P1}^{(l,i)} & \dots & \boldsymbol{j}_{Pi}^{(l,i)} & \boldsymbol{0} & \dots & \boldsymbol{0} \end{bmatrix} \tag{10}$$

$$\boldsymbol{J}_O^{(l,i)} = \begin{bmatrix} \boldsymbol{j}_{O1}^{(l,i)} & \dots & \boldsymbol{j}_{Oi}^{(l,i)} & \boldsymbol{0} & \dots & \boldsymbol{0} \end{bmatrix} \tag{11}$$

the columns of the matrices in (10) and (11) can be computed as follows:

$$\boldsymbol{j}_{Pj}^{(l,i)} = \begin{cases} \boldsymbol{z}_{j-1} & \text{for a prismatic joint} \\ \boldsymbol{z}_{j-1} \times (\boldsymbol{p}_{\ell_i} - \boldsymbol{p}_{j-1}) & \text{for a revolute joint} \end{cases} \tag{12}$$

$$\boldsymbol{j}_{Oj}^{(l,i)} = \begin{cases} \boldsymbol{0} & \text{for a prismatic joint} \\ \boldsymbol{z}_{j-1} & \text{for a revolute joint} \end{cases} \tag{13}$$

where $\boldsymbol{p}_{j-1}$ and $\boldsymbol{z}_{j-1}$ are the position vector of the origin and the unit vector of the axis z of the frame of the $(j-1)$-th joint, respectively, and $\boldsymbol{p}_{\ell_i}$ is the position of the CoM of the i-th link.

The full model is the most common model used in robotics to calculate the mass matrix of the system. However, the definition of parameters m_i and $\boldsymbol{I}_i$ is usually difficult starting from the manuals and the datasheets given by the robot manufacturers. An estimation of such parameters can be obtained using CAD models [20] or through extensive experimental tests [21–23].

2.2. Simplified model

The simplified model is an approximated model based on the approach presented in [17]. It simplifies the mass distribution of the robot considering only two lumped masses for each link placed in such a way that the link mass m_i and its CoM position are preserved, whereas the inertia tensor generally is not kept constant. The link reference frames are defined according to the Denavit–Hartenberg convention, and the lumped masses are placed along the z_i and z_{i+1} axes at appropriate distances from the link origins. It is worth noting that, although the link mass and the CoM position are derived from the CAD models,

https://doi.org/10.1017/S0263574726103713 Published online by Cambridge University Press

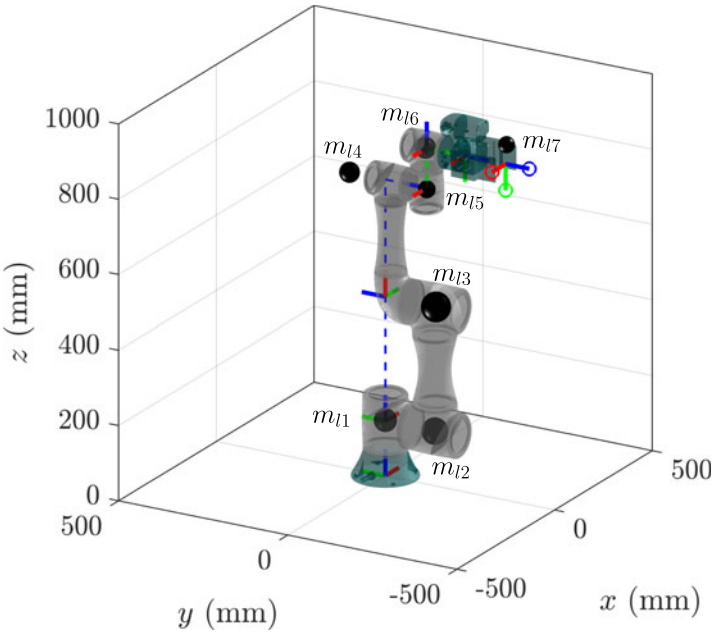


Figure 1. *Position of the aggregated lumped masses (black spheres) in the robotic manipulator TechMan TM5-700.*

they are less influenced by the actual shape of the link internals, as the inertia tensor; hence, they are "robust" quantities.

In the simplified model, the number of lumped masses is equal to twice the number of links. Very often, some lumped masses are placed in the same position, thus they can be aggregated [17].

The mass matrix of the simplified model can be calculated via the Lagrangian approach, in which only the linear velocities of the aggregated lumped masses have to be computed; this leads to a reduction in computational time [16, 17]. The mass matrix can be calculated as:

$$\boldsymbol{M}(\boldsymbol{q}) = \sum_{i=2}^{N} \left(m_{l,i} \boldsymbol{J}_P^{(l,i)T} \boldsymbol{J}_P^{(l,i)} \right) \tag{14}$$

where $m_{l,i}$ is the i-th aggregated mass, $\boldsymbol{J}_P^{(l,i)}$ is the Jacobian that links the joint velocities and the linear velocities of the i-th aggregated mass, and $N \leq 2n$ is the total number of masses used to describe the system. Please note that the sum of Eq. (14) starts from 2 since one of the two masses of link 1 must be placed on the first axis, thus its linear velocity is zero.[2]

As an example, in Figure 1, the distribution of the aggregated lumped masses $m_{l,i}$ of a robotic manipulator, the TechMan TM5-700, is illustrated. The simplified model consists of seven masses, of which the first is steady since it is placed on the z_1 axis. Hence, the full model, which is made of 6 masses and 6 inertia tensors, is reduced to a simplified model made of only 7 lumped masses.

2.3. Standard model

The ISO 10218-2:2025 standard [6] establishes the safety requirements for the installation and use of industrial robots in collaborative applications. In fact, unlike traditional robots, which must be used

[2] This assumption is true if the first joint is a revolute joint; on the other hand, if the first joint is prismatic also the first mass has a non-null linear velocity.

https://doi.org/10.1017/S0263574726103713 Published online by Cambridge University Press

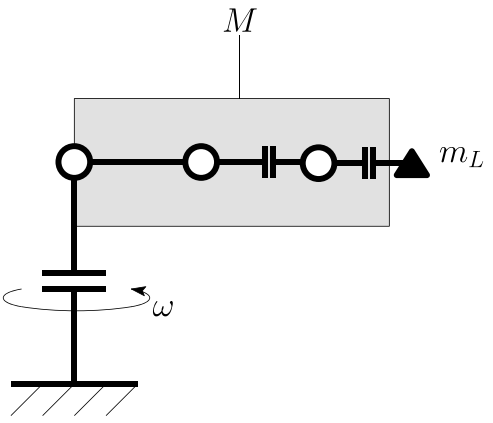


Figure 2. *Simplified mass distribution model in the ISO/TS 15066:2016 standard [7].*

within safety zones that separate the operator from the manipulator, collaborative robots are designed to allow safe interaction with people [24].

According to the ISO standard, the kinetic energy of the two impacting bodies before the impact can be equated to the elastic energy accumulated within the materials in contact during the impact:

$$E_k = \frac{F^2}{2k} = \frac{1}{2}\mu v_{rel}^2 \tag{15}$$

where E_k represents the exchanged kinetic energy, F is the elastic contact force, k is the effective spring constant [7] of the materials in contact,[3] v_{rel} is the relative velocity of the bodies along the normal to the plane tangent to the two colliding surfaces $\boldsymbol{n}$, and μ is the reduced mass of the robot-operator system and is determined using the following formula:

$$\mu = \left(\frac{1}{m_H} + \frac{1}{m_R}\right)^{-1} \tag{16}$$

in which m_H represents the effective mass of the body part subjected to impact,[4] while m_R represents the effective mass of the robot, calculated according to ISO 10218-2:2025 as follows:

$$m_R = \frac{M}{2} + m_L \tag{17}$$

where M is the total mass of the moving parts of the robot and m_L is the payload, including the end-effector and the workpiece (Figure 2).

3. Effective mass for a SCARA robot

The proposed model is applied to the SCARA Omron i4-550L robot. First, using the method described in [17], the lumped parameter model of the robot is derived.

3.1. Lumped parameter model

The DH parameters are reported in Table I, while the controlled joint variables $q_1, \ldots, q_4$ are represented in Figure 3 and collected in vector $\boldsymbol{q}$. The mass and the position of the COM of each link have been

[3] The ISO 10218-2:2025 standard provides a list of stiffnesses of the body parts to which the robot is colliding, and it assumes that the stiffness of the material of the body part is much lower than that of the robot.

[4] The ISO 10218-2:2025 standard provides a list of masses of the body parts to which the robot is colliding.

https://doi.org/10.1017/S0263574726103713 Published online by Cambridge University Press

Table I. *DH parameters of the links of the Omron i4-550L.*

Link i	$\boldsymbol{\alpha_{i-1}}$ (°)	$\boldsymbol{a_{i-1}}$ **(mm)**	$\boldsymbol{\theta_i}$ (°)	$\boldsymbol{d_i}$ **(mm)**
1	0	0	q_1	270
2	0	275	q_2	80
3	180	275	0	q_3
4	0	0	q_4	0

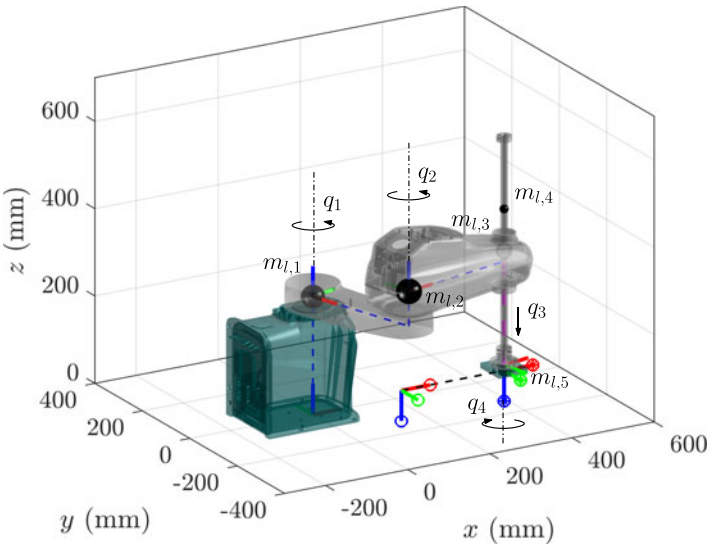


Figure 3. *Position of the aggregated lumped masses (black spheres) in the SCARA Omron i4-550L and a sample impact trajectory marked with a dashed black line.*

estimated by means of a CAD software [20]. In Table II, the total mass m_i of each link and the values of the four parameters of the calculated lumped mass model are presented.

O_i and O_{i+1} are the origins of the frames of link i and $i+1$, respectively. L_{1i} is the position of the mass m_{1i} measured from O_i along the z_i axis, while L_{2i} is the position of the mass m_{2i} measured from the intersection point between the z_{i+1} and x_i axes along the z_{i+1} axis. The two quantities are defined according to the corresponding axis directions and can therefore assume both positive and negative values. The parameters $\kappa_{1i} = \frac{m_{1i}}{m_i}$ and $\kappa_{2i} = \frac{m_{2i}}{m_i}$ are the two normalized lumped masses defined such that their sum is 1.

The two masses located at the same point, but coming from the lumped parameter representation of two adjacent links, can be aggregated together. After this operation, the aggregated lumped masses are

$$m_{l,1} = \kappa_{11} m_1 \tag{18}$$

$$m_{l,2} = \kappa_{21} m_1 + \kappa_{12} m_2 \tag{19}$$

$$m_{l,3} = \kappa_{22} m_2 \tag{20}$$

$$m_{l,4} = \kappa_{13} m_3 + \kappa_{14} m_4 \tag{21}$$

$$m_{l,5} = \kappa_{23} m_3 + \kappa_{24} m_4 \tag{22}$$

Overall, the simplified model consists of 5 aggregated lumped masses as shown in Figure 3, the first is steady (as it belongs to the z_1 axis) and the other four are mobile. This is an important simplification

https://doi.org/10.1017/S0263574726103713 Published online by Cambridge University Press

Table II. *Lumped parameters of the links of the Omron i4-550L.*

Link i	m_i **(kg)**	L_{1i} **(mm)**	L_{2i} **(mm)**	κ_{1i} ()	κ_{2i} ()
1	3.38	−55	80	0.556	0.444
2	1.49	0	−25	0.588	0.412
3	0.19	−358	12	0.500	0.500
4	0.16	−358	12	0.017	0.983

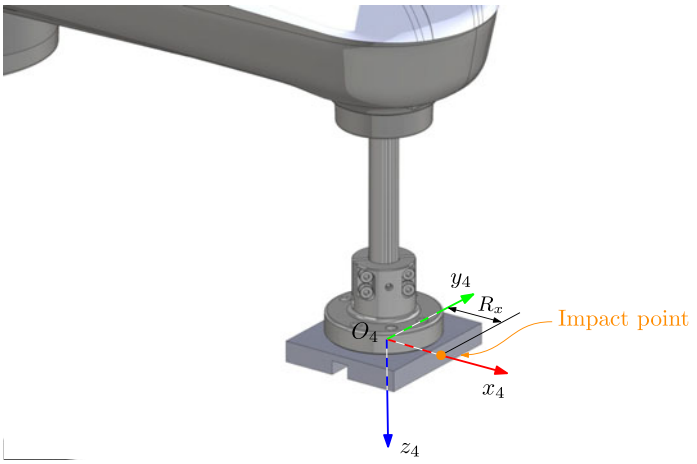


Figure 4. *Impact point and its distance from the tool reference system.*

because in this way the inertia model is composed of only 5 aggregated lumped masses instead of 4 masses and 4 inertia tensors.

3.2. Effective mass

We apply Equations from (3) to (8) to compute the effective mass for both the full and the simplified SCARA models. Before proceeding, the Jacobian matrix and the mass matrix are defined for each model.

The Jacobian matrix is evaluated at the impact point, located at a distance R_x from the origin O_4 of the tool reference frame along the x_4 axis (Figure 4). The impact direction always coincides with x_4.

The Jacobian matrix is the same for both models, and it is [25]:

$$\boldsymbol{J}(\boldsymbol{q}) = \begin{bmatrix} -l_1 \sin(q_1) - l_2 \sin(q_1+q_2) + J_1 & -l_2 \sin(q_1+q_2) + J_1 & 0 & -J_1 \\ l_1 \cos(q_1) + l_2 \cos(q_1+q_2) + J_2 & l_2 \cos(q_1+q_2) + J_2 & 0 & -J_2 \\ 0 & 0 & -1 & 0 \\ 0 & 0 & 0 & 0 \\ 0 & 0 & 0 & 0 \\ 1 & 1 & 0 & -1 \end{bmatrix} \tag{23}$$

where

$J_1 = -R_x \sin(q_1 + q_2 - q_4)$

$J_2 = R_x \cos(q_1 + q_2 - q_4)$

Planar impacts are considered. On the one hand, the orientation of the normal direction with respect to the fixed frame is ϕ. On the other hand, normal direction passing through the kinetic chain is

https://doi.org/10.1017/S0263574726103713 Published online by Cambridge University Press

$q_1 + q_2 - q_4$. Therefore, the following orientation equation holds:

$$\phi = q_1 + q_2 - q_4 \tag{24}$$

and q_4 in Eq. (23) is not an independent variable.

The mass matrix depends on the inertia parameters and is therefore different for the two models. For the full model, the mass matrix is given by:

$$\boldsymbol{M}(\boldsymbol{q}) = \begin{bmatrix} M_{11} & M_{12} & 0 & -I_4 \\ M_{12} & M_{22} & 0 & -I_4 \\ 0 & 0 & m_3 + m_4 & 0 \\ -I_4 & -I_4 & 0 & I_4 \end{bmatrix} \tag{25}$$

where

$M_{11} = m_1 r_1^2 + m_2(l_1^2 + r_2^2) + 2m_2 l_1 r_2 \cos(q_2) + I_1 + I_2 + I_3 + I_4 + (m_3 + m_4)(l_1^2 + 2l_1 l_2 \cos(q_2) + l_2^2)$

$M_{12} = m_2(r_2^2 + l_1 r_2 \cos(q_2)) + I_2 + I_3 + I_4 + (m_3 + m_4)(l_1 l_2 \cos(q_2) + l_2^2)$

$M_{22} = m_2 r_2^2 + I_2 + I_3 + I_4 + (m_3 + m_4) l_2^2$

and l_i is the distance between origins O_i and O_{i+1}, and r_i is the distance of the i-th CoM to the origin O_i.

In the simplified model, the mass matrix becomes a 3×3 matrix because, due to the placement of the lumped masses of the last link along the axis of the third joint (see Figure 3), the kinetic energy of the robot does not depend on q_4. As a result, the Jacobian matrix should be considered with only three columns when computing the effective mass using Eq. (4). In this case, the mass matrix becomes

$$\boldsymbol{M}(\boldsymbol{q}) = \begin{bmatrix} M_2 l_1^2 + M_3(l_1^2 + 2l_1 l_2 \cos(q_2) + l_2^2) & M_3(l_1 l_2 \cos(q_2) + l_2^2) & 0 \\ M_3(l_1 l_2 \cos(q_2) + l_2^2) & M_3 l_2^2 & 0 \\ 0 & 0 & m_{l,4} + m_{l,5} \end{bmatrix} \tag{26}$$

where

$M_2 = m_{l,2}$

$M_3 = m_{l,3} + m_{l,4} + m_{l,5}$

Neglecting the motion along the z axis, the behavior of the SCARA robot becomes that of a planar mechanism. Consequently, the aggregate masses M_2 and M_3 represent, respectively, the mass concentrated in the elbow and the mass concentrated in the end-effector of the equivalent planar mechanism (Figure 5). The mass $M_1 = m_{l,1}$, positioned along the z_1 axis, is not considered in the calculation of the mass matrix $\boldsymbol{M}(\boldsymbol{q})$, since it does not participate in the planar motion of the robot.

Given a normal direction $\boldsymbol{n}$, the calculation of m_n is performed using the Equations from (3) to (8). In the case here considered, the normal direction $\boldsymbol{n}$ lies in the horizontal plane, and the effective mass is always independent of q_3, that is, of movement along the z axis.

In the case here considered, the normal direction $\boldsymbol{n}$, perpendicular to the plane tangent to the impact point, is aligned with the x_4 axis, since the contact surface is orthogonal to x_4. If this condition does not hold, that is, if the surface is inclined with respect to the x_4 direction, then the inclination angle of the impact surface relative to x_4 must be taken into account in the orientation Eq. (24).

By substituting Eq. (24) into the Jacobian matrix, the effective mass $m_{n,f}$ for the full model becomes:

$$m_{n,f} = \frac{-(M_{12}^2 - 2I_4 M_{12} + I_4 M_{11} + I_4 M_{22} - M_{11} M_{22})}{(M_{11} - 2M_{12} + M_{22}) l_2^2 \sin^2(q_1 + q_2 - \phi) + (M_{22} - I_4) l_1^2 \sin^2(q_1 - \phi) + 2(M_{22} - M_{12}) l_1 l_2 \sin(q_1 + q_2 - \phi) \sin(q_1 - \phi)} \tag{27}$$

While for the simplified model the effective mass $m_{n,s}$ is

$$m_{n,s} = \frac{M_3 \left(M_3 \sin^2(q_2) + M_2\right)}{M_3 \sin^2(q_2) + M_2 \sin^2(q_1 + q_2 - \phi)} \tag{28}$$

https://doi.org/10.1017/S0263574726103713 Published online by Cambridge University Press

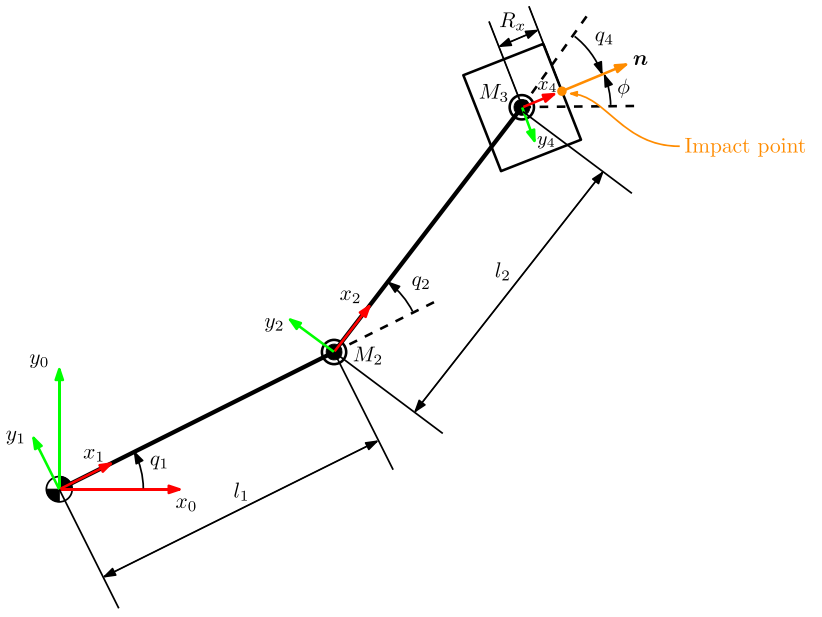


Figure 5. *Schematic SCARA model with impact point and normal direction* $\boldsymbol{n}$.

If the normal direction $\boldsymbol{n}$ coincides with the axes $\boldsymbol{x}$ or $\boldsymbol{y}$, the calculus of the effective mass is even easier. For the x-direction $\boldsymbol{n} = [1\ 0\ 0]^T$, the rotation angle ϕ is equal to 0, while for the y-direction $\boldsymbol{n} = [0\ 1\ 0]^T$, the rotation angle ϕ is equal to $\frac{\pi}{2}$.

For the ISO standard model, the effective mass m_R is given, as mentioned in Eq. (17), by:

$$m_R = \frac{M}{2} + m_L = \frac{\sum_i m_i}{2} + m_L \tag{29}$$

where m_L is the mass of the end-effector, since there is no workpiece.

4. Comparison between the models

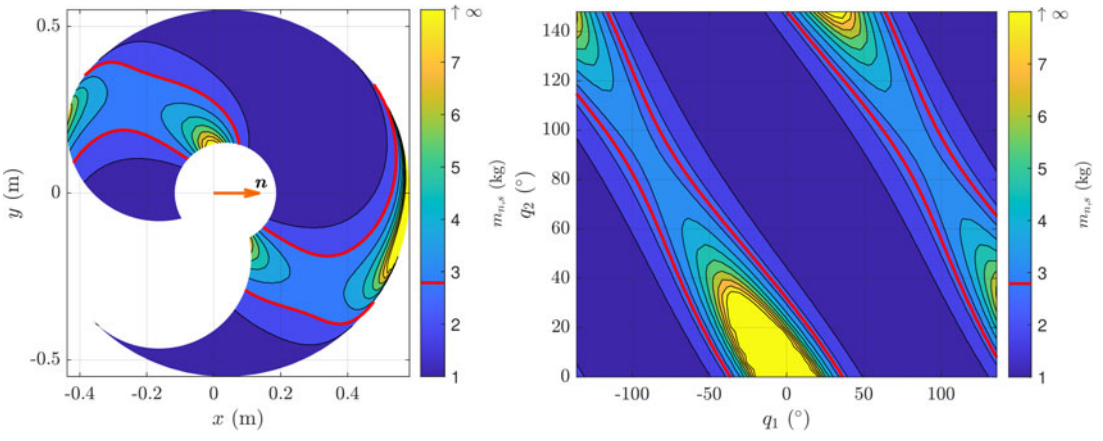
In this section, the impact direction ϕ is kept constant, and the effect of the robot configuration is analyzed. Robot configuration determines the position of the impact point in the Cartesian space. The SCARA robot in the right-arm configuration (with joint 2 on the right side of the line connecting joints 1 and 4) is considered.

4.1. Comparison of effective mass

Equation (28) shows that the effective mass depends only on q_1 and q_2. The values of the aggregated masses M_2 and M_3 of the equivalent planar mechanism are 2.38 and 0.97 kg, respectively, while the joint ranges for the first two joints are $\pm 136^\circ$ and $\pm 148^\circ$, respectively. The value of the mass for the ISO standard model is $m_R = 2.77$ kg. Figure 6 shows the values of the effective mass given by the simplified model in the Cartesian and joint spaces when the impact direction coincides with the x_0 axis ($\phi = 0$). The red lines indicate the contours where the effective mass is equal to the ISO standard value m_R.

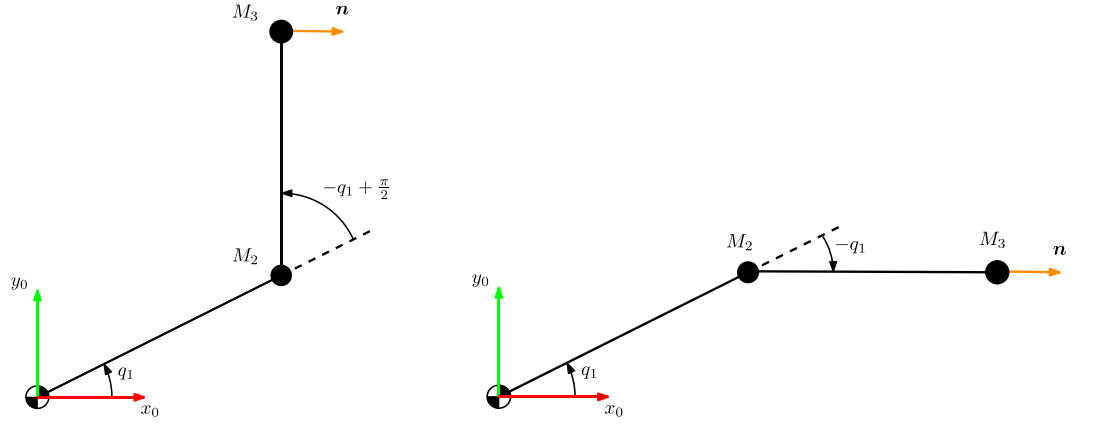
The plots were generated by linearly discretizing the ranges of the angles q_1 and q_2 into 50 intervals each. For improved visual interpretation, the data were represented using contour (isoline) regions. The two graphs show that the minima and maxima do not occur at isolated points, but extend along curved trajectories in the Cartesian and joint space. In particular, the minimum values of $m_{x,s}$ occur when $q_2 = -q_1 + \phi + \frac{\pi}{2}$. By substituting this relation, it follows that $m_{n,s} = M_3$. This particular condition corresponds to a specific configuration of the robot, in which the second link remains always

https://doi.org/10.1017/S0263574726103713 Published online by Cambridge University Press



(a) (b)

Figure 6. *Values of the effective mass given by the simplified model in the Cartesian space (a) and in the joint space (b) with* $\boldsymbol{n} = [1\ 0\ 0]^T$. *The red curves represent the reduced mass calculated according to the ISO standard.*



(a) (b)

Figure 7. *Schematic representation of the SCARA robot in configuration of minimum effective mass (a) and maximum effective mass (b) with* $\boldsymbol{n} = [1\ 0\ 0]^T$ *and* $\phi = 0$.

perpendicular to the normal direction of impact. In this configuration, only the aggregated mass M_3 contributes to the impact as shown in Figure 7(a).

In contrast, the second link of the robot remains parallel to the direction of impact (see Figure 7(b)) when $q_2 = -q_1 + \phi$. In this configuration, the effective mass reaches the maximum value, which is a function of q_2:

$$m_{n,s} = M_3 + \frac{M_2}{\sin(q_2)^2} \tag{30}$$

If $\phi = 0$ and $q_1 = 0$, q_2 becomes 0 and the robot reaches a singularity in the normal direction $\boldsymbol{n}$, and, for this reason, the effective mass tends to infinity.

To further analyze the effect of robot configuration on the value of the effective mass, the diagram in Figure 8 shows the probability density of the values of the effective mass of the SCARA robot. The diagram is calculated considering 2500 robot configurations corresponding to 2500 end-effector locations uniformly distributed on the workspace. In the diagram, the mean, the median value, and the ISO standard value are reported as well. A bimodal distribution is observed. The value proposed by the

https://doi.org/10.1017/S0263574726103713 Published online by Cambridge University Press

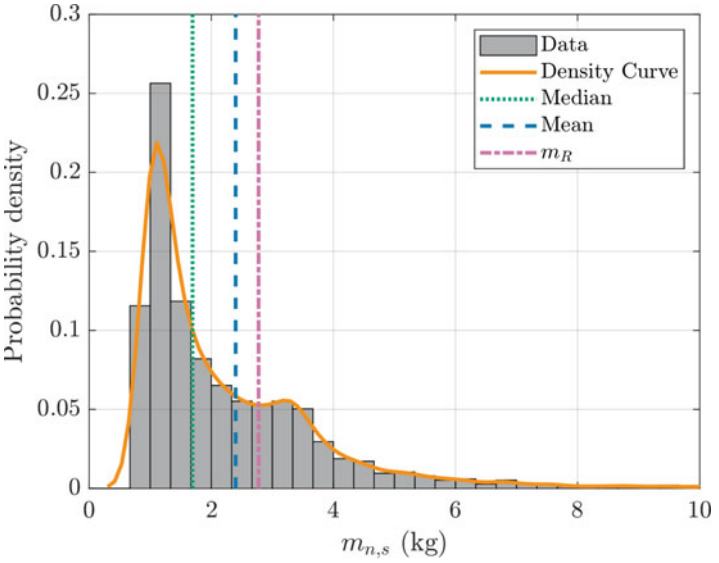
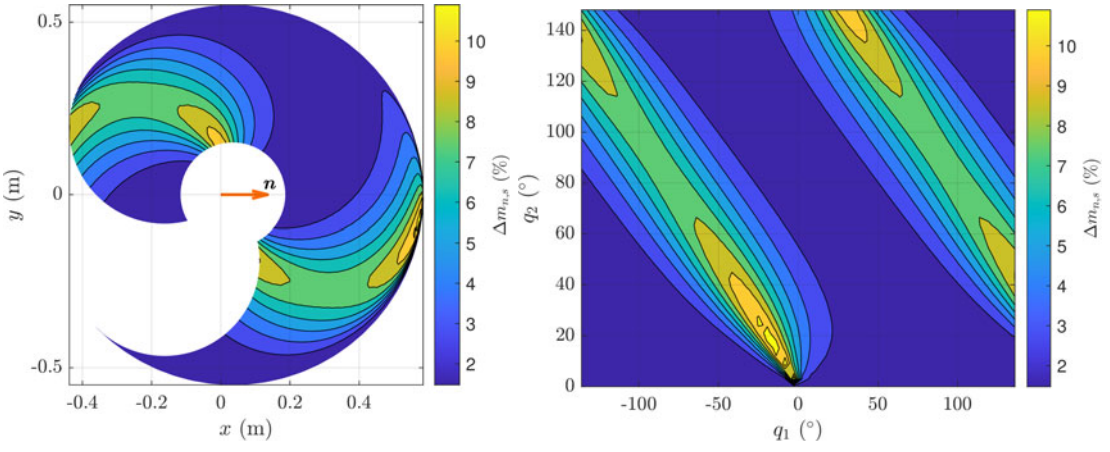


Figure 8. *Probability density of the values of the effective mass in the simplified model with* $\boldsymbol{n} = [1\ 0\ 0]^T$.



(a) (b)

Figure 9. *Percentage relative error in effective mass between the full model and the simplified model in the Cartesian space (a) and joint space (b) with* $\boldsymbol{n} = [1\ 0\ 0]^T$.

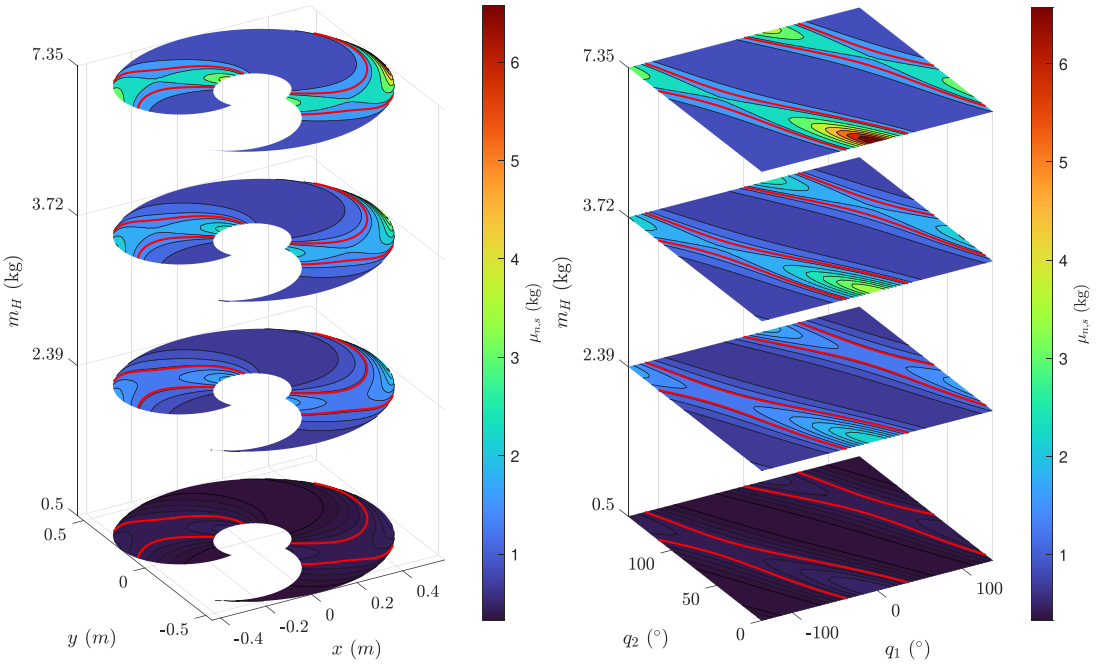
ISO standard m_R overestimates both the mean and the median. In particular, more than 70% of the values are less than the ISO standard value, highlighting the conservative nature of the ISO standard, which prioritizes safety.

In order to compare the proposed simplified model with the full model, the relative errors in effective mass are calculated. The graphs in Figure 9 represent the percentage relative errors in effective mass ($\Delta m_{n,s}$) in the Cartesian and joint space. It can be seen that the error in the worst case reaches 10%. However, in 75% of the cases, the error does not exceed 6%, indicating a good level of accuracy for the simplified lumped parameter model.

4.2. Comparison of reduced mass

The kinetic energy calculated by the ISO standard in Eq. (15) is the relative kinetic energy of the system before the impact. Introducing Eq. (16) in Eq. (15) the ISO standard energy can be expressed as a

https://doi.org/10.1017/S0263574726103713 Published online by Cambridge University Press



(a) (b)

Figure 10. *Values of the reduced mass of the simplified model in the Cartesian space (a) and joint space (b) with* $\boldsymbol{n} = [1\ 0\ 0]^T$ *for 4 different values of obstacle mass. The red curves represent the reduced masses calculated according to the ISO standard.*

function of robot effective mass of the ISO standard m_R and obstacle mass m_H:

$$E_{k,\mathrm{ISO}} = \frac{1}{2}\frac{m_R m_H}{m_R + m_H}(v_{1n} - v_{2n})^2 = \frac{1}{2}\mu_{\mathrm{ISO}} v_{rel}^2 \tag{31}$$

where μ_{ISO} is the reduced mass according to the ISO standard.

In order to compare the ISO standard with both the full and the simplified models, the relative kinetic energy before impact can be calculated simply substituting in Eq. (31) m_R with the effective masses predicted by the full and simplified models:

$$E_{k,f} = \frac{1}{2}\frac{m_{n,f} m_H}{m_{n,f} + m_H}(v_{1n} - v_{2n})^2 = \frac{1}{2}\mu_{n,f} v_{rel}^2 \tag{32}$$

$$E_{k,s} = \frac{1}{2}\frac{m_{n,s} m_H}{m_{n,s} + m_H}(v_{1n} - v_{2n})^2 = \frac{1}{2}\mu_{n,s} v_{rel}^2 \tag{33}$$

where $m_{n,f}$ and $m_{n,s}$ are the effective mass and $\mu_{n,f}$ and $\mu_{n,s}$ the reduced masses for full and simplified models along the normal direction, respectively.

Since the kinetic energy depends only on the reduced mass and relative velocity, comparing the reduced masses is sufficient to evaluate the kinetic energies estimated by the two models. The relationship between the reduced mass and the obstacle mass is such that, when $m_{n,f} \to \infty$ (or $m_{n,s} \to \infty$), it follows that $\mu_{n,f} = m_H$ (or $\mu_{n,s} = m_H$). This is a relevant observation because, unlike the effective mass, the reduced mass never diverges.

A set of obstacle mass values was selected to analyze and represent the behavior of the reduced mass in both Cartesian and joint spaces. The selected obstacle masses are 0.5, 2.39, 3.72, and 7.35 kg, corresponding to the values used in the experimental tests. Figure 10 shows the values of the reduced mass

https://doi.org/10.1017/S0263574726103713 Published online by Cambridge University Press

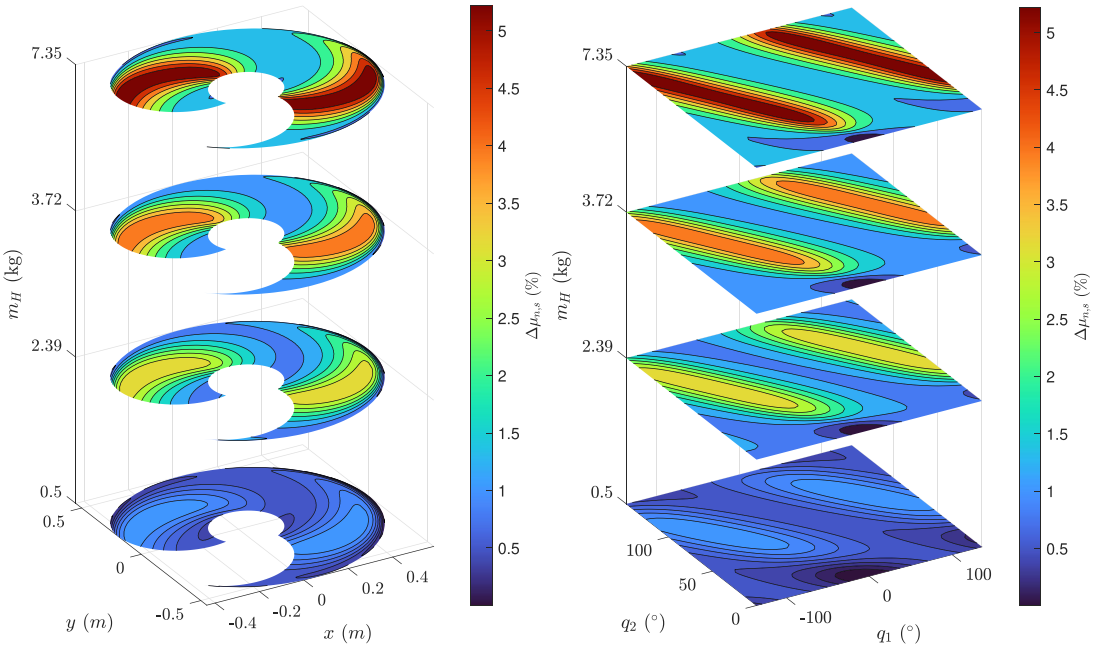


Figure 11. *Percentage relative error in reduced mass between the full model and the simplified model in the Cartesian space (a) and joint space (b) with* $\boldsymbol{n} = [1\ 0\ 0]^T$ *for 4 different values of obstacle mass.*

calculated by means of the simplified model. The values of the ISO standard model μ_{ISO} (shown in red) corresponding to the four obstacle masses are 0.42, 1.28, 1.59, and 2.01 kg. The red lines in Figure 10 represent the contours where the reduced mass is equal to the ISO standard value μ_{ISO}. It can be observed that for small obstacle masses, the range of variation $\mu_{n,s}$ is narrower.

The graphs in Figure 11 represent the percentage relative errors in reduced mass ($\Delta\mu_{n,s}$) between the full and simplified model in the Cartesian and joint space. It can also be seen that in the worst cases, the errors are at most 5%, highlighting the good approximation of the simplified lumped parameter model.

All the previously reported results dealt with impacts in x direction. The analysis of the effect of impact direction was carried out considering the simplified model and $m_H = 2.39$ kg as a representative case. The values of the reduced masses $\mu_{n,s}$ for the normal direction y and a generic direction in the Cartesian space are depicted in Figure 12.

The plots are equal to the one obtained for $\boldsymbol{n} = [1\ 0\ 0]^T$, but are rotated in the Cartesian space by an angle corresponding to the rotation ϕ. As shown in Figure 13, rotating the impact direction by 90° (from the x direction to the y direction) results in an equivalent configuration along the new normal direction, provided that the joint coordinate q_1 is also increased by 90°. This implies that varying the orientation of the normal direction causes the effective mass values to rotate accordingly, producing plots that retain their shape but appear rotated in Cartesian space.

Finally, the effect of the left-arm configuration of the SCARA robot is considered. The results presented in Figure 14 show symmetry with respect to the normal direction, reflecting the intrinsic symmetry of the configuration.

Since there is an overlap between the workspaces attainable with left- and right-arm configurations, the configuration that minimizes the reduced mass can be chosen. Figure 15 represents the reduced mass in the Cartesian space, considering the minimum values calculated from the two configurations.

https://doi.org/10.1017/S0263574726103713 Published online by Cambridge University Press

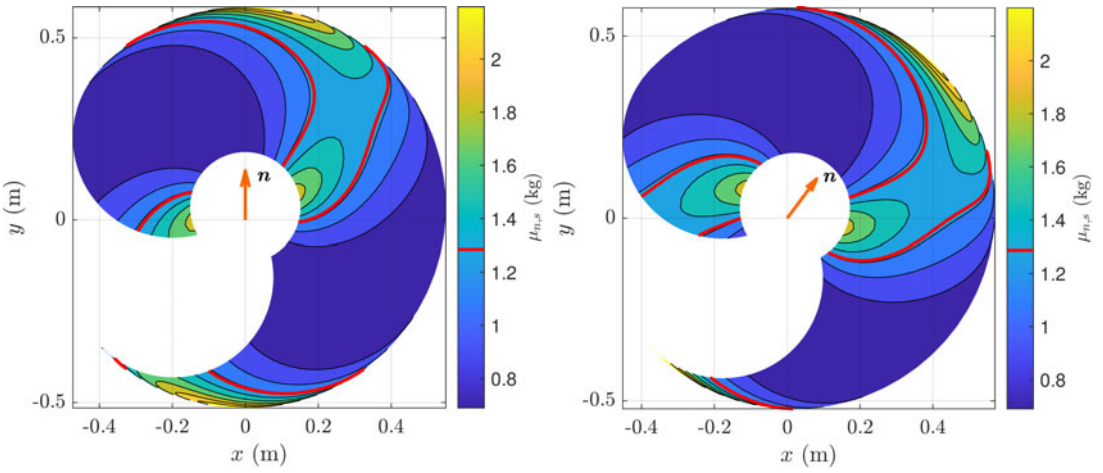


Figure 12. *Values of the reduced mass of the simplified model in Cartesian space with* $\boldsymbol{n} = [0\ 1\ 0]^T$ *(a) and with* $\boldsymbol{n} = [0.6\ 0.8\ 0]^T$ *(b). The red curves represent the reduced mass calculated according to the ISO standard.*

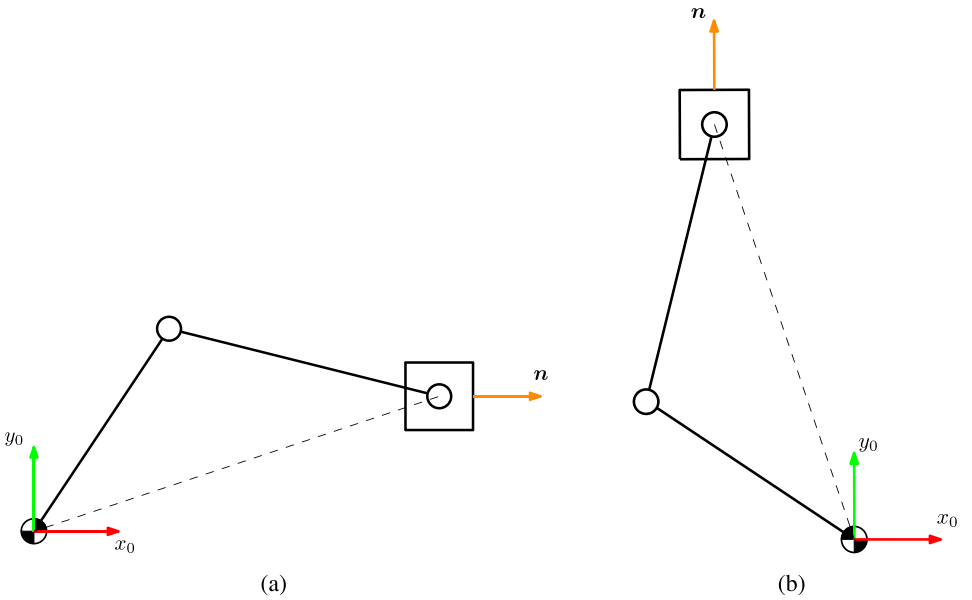


Figure 13. *Schematic representation of a SCARA robot with the same configuration according to the x normal direction (a) and y normal direction (b).*

5. Experimental setup and validation

This section describes the experimental setup used to validate the theoretical results obtained with the proposed simplified model. The aim is to perform the same impact test in different robot configurations to evaluate the effect of variation in the effective mass and, in turn, on the reduced mass. According to Eq. (15) of the ISO standard, the impact force was measured by means of a load cell to compare the force with the estimated reduced masses. In fact, until the relative velocity v_{rel} and the spring constant k are kept constant, the square of the impact force must be proportional to the reduced mass μ.

https://doi.org/10.1017/S0263574726103713 Published online by Cambridge University Press

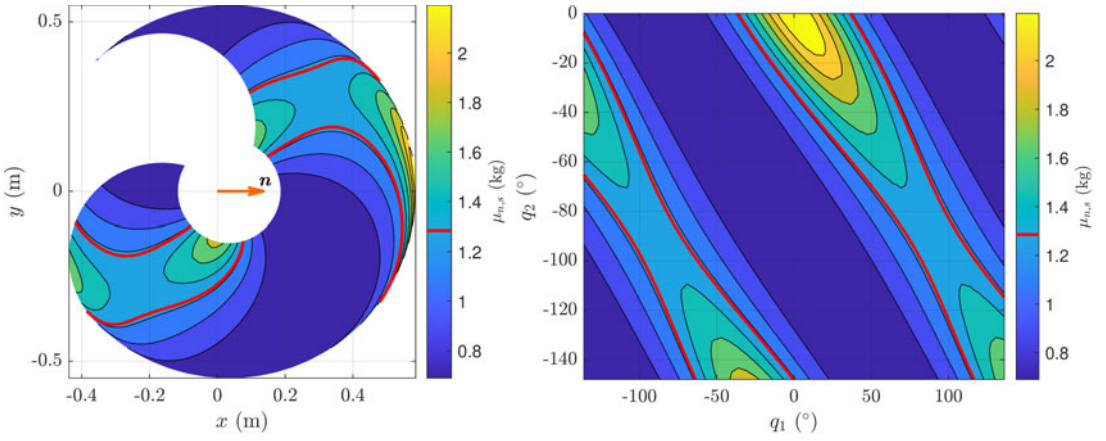


Figure 14. *Values of the reduced mass of the simplified model in the Cartesian space (a) and joint space (b) with* $\boldsymbol{n} = [1\ 0\ 0]^T$ *with left-arm configuration. The red curves represent the reduced mass calculated according to the ISO standard.*

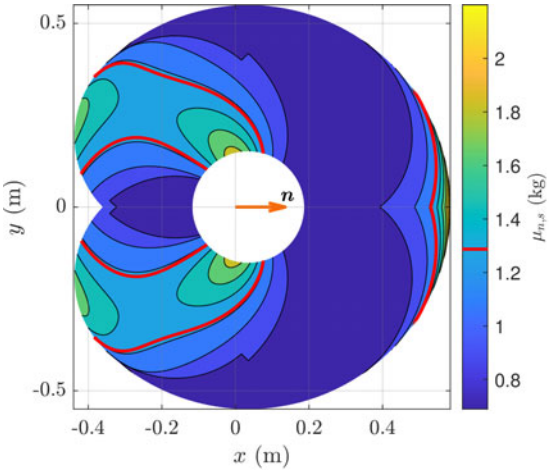


Figure 15. *Values of the minimum reduced mass of the simplified model in the Cartesian space with* $\boldsymbol{n} = [1\ 0\ 0]^T$ *in the two configurations. The red curves represent the reduced mass calculated according to the ISO standard.*

The experimental setup consists of an Omron i4-550L SCARA robot and a sliding bearing carriage mounted on an MISUMI linear guide. The data acquisition system includes a PCB Piezotronics quartz force sensor 208C03 with a sensitivity of 2.224 mV/kN, a National Instruments module NI-9230, and a data acquisition chassis NI cDAQ-9174. Data were acquired at a sampling rate of 12,800 Hz for a total of 10,000 samples.

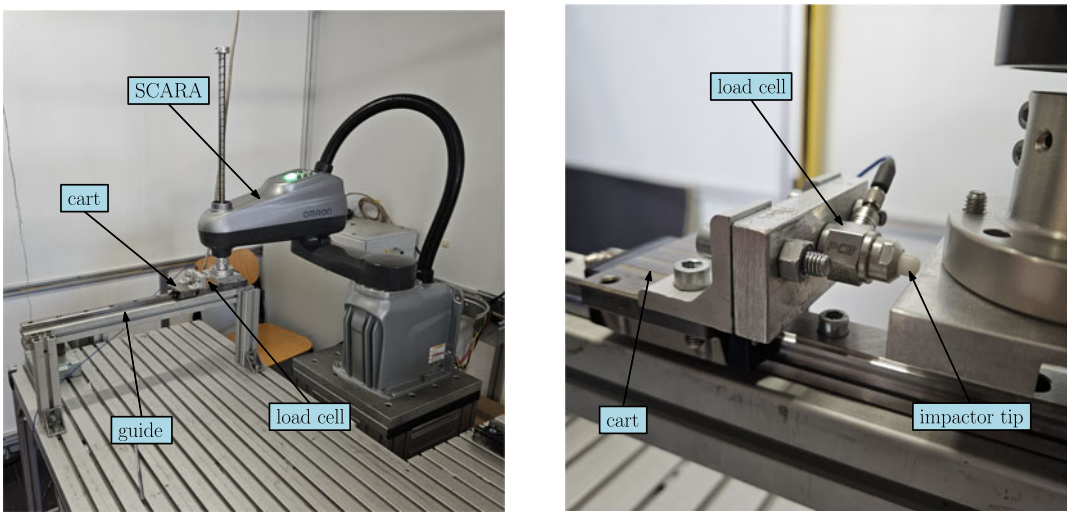
The experimental tests consist of impacting the SCARA robot with the sliding cart (Figure 16(a)) and measuring the impact force through the load cell (Figure 16(b)). In particular, three different robot configurations and impact points were selected, each corresponding to a different value of effective mass (calculated with Eq. (28) of the simplified model), as shown in Table III.

The tests were carried out at a constant velocity of 250 mm/s with the robot in right arm configuration. The two materials in contact were aluminum and high-density polyethylene (HDPE); in particular, an impactor HDPE tip was mounted on the load cell (see Figure 16(b)), and an aluminum plate was fixed

https://doi.org/10.1017/S0263574726103713 Published online by Cambridge University Press

Table III. *Test points in Cartesian coordinates and correspondent values of effective mass.*

Conf.	x (mm)	y (mm)	$m_{n,s}$ (kg)
1	300	200	0.97
2	300	−100	1.82
3	300	−250	3.32



(a) (b)

Figure 16. *Experimental setup with SCARA Omron i4-550L robot and the sliding carriage (a) and the load cell with the impactor tip (b).*

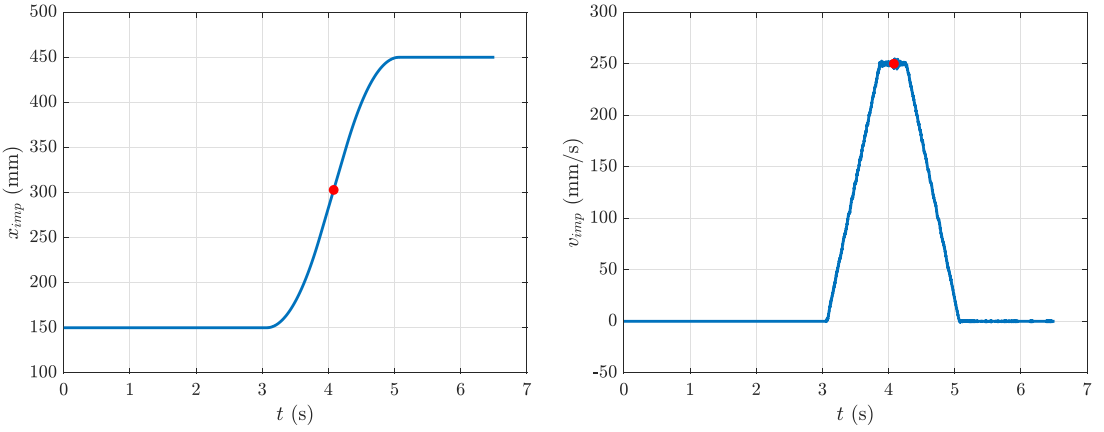
to the robot. The independent joint variable q_3 was set equal to 236 mm. In this way, a common contact scenario is replicated that typically occurs when the third link is in an elevated position during motion. The value of the reduced mass depends not only on the effective mass, that is, the robot configuration, but also on the obstacle mass m_H as shown in Eq. (16). For this reason, the tests were carried out with four different values of m_H: 0.50, 2.39, 3.72, and 7.35 kg.

The tests were carried out by imposing a linear trajectory of the tool along the guide axis. A constant tool velocity was obtained because a trapezoidal velocity profile was implemented, and the impact occurred at the midpoint of the trajectory. As an example, Figure 17 shows the position and velocity of the tool along the x-axis when the impact occurs in position (300, 200). These data were obtained by collecting the joint positions and velocities from the robot control software.

For each configuration and each obstacle mass, three impact tests were performed, and the corresponding impact forces were recorded over time. As an example, Figure 18 shows the impact force trends for each configuration with $m_H = 2.39$ kg. We can see that the tests are highly repeatable; for this reason, we carried out only three tests per case. The oscillations in the force are due to the end-effector vibrations against the impactor tip during contact. Similar results were obtained in a previous research presented in [26].

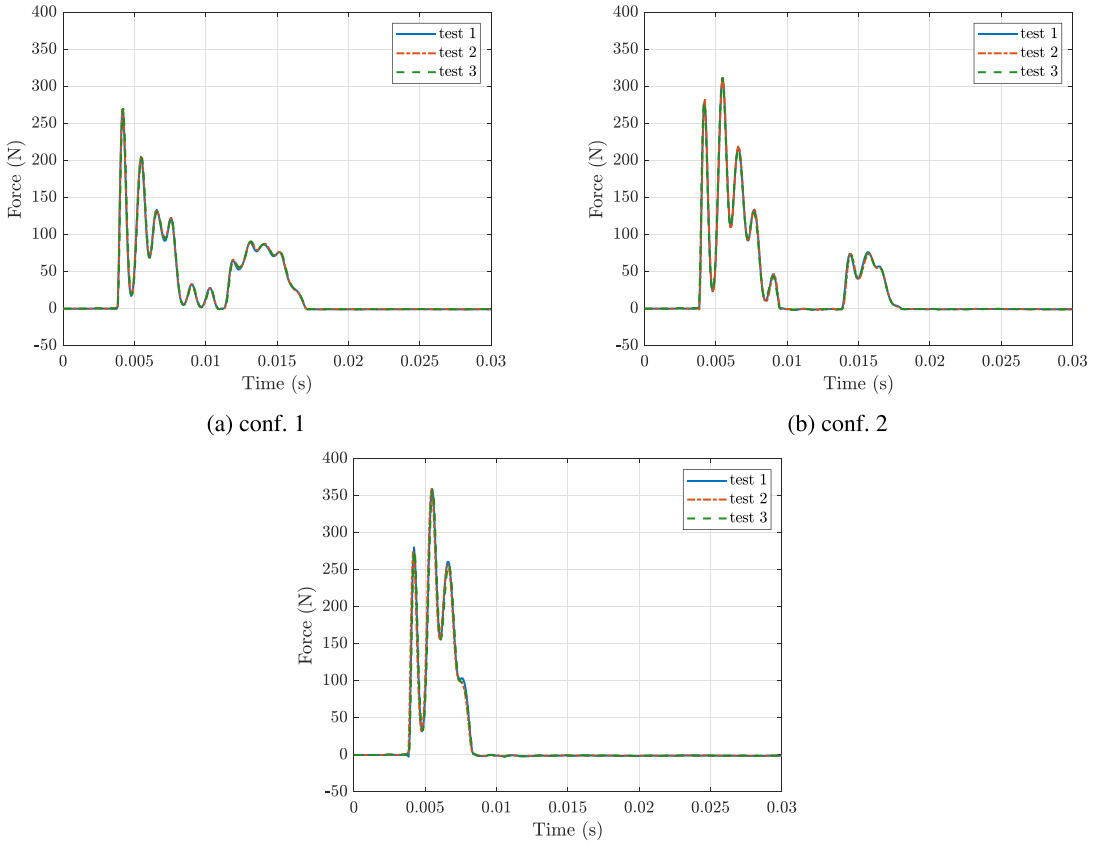
For each case, the mean maximum force was calculated. Figure 19(a) shows the effect of configuration and obstacle mass on the mean maximum forces obtained from the experimental tests. Figure 19(b) shows the theoretical trends predicted by the simplified lumped parameter model. In fact, from Eq. (15) it follows that, for a given velocity, the experimentally measured impact force is proportional to the

https://doi.org/10.1017/S0263574726103713 Published online by Cambridge University Press



(a) (b)

Figure 17. *Position (a) and velocity (b) of the tool along the x coordinate when the impact occurs in position (300, 200) and an impact velocity of 250 mm/s. In red, the instant of impact is presented.*



(a) conf. 1 (b) conf. 2

(c) conf. 3

Figure 18. *Force trends for each configuration with $m_H = 2.39$ kg.*

https://doi.org/10.1017/S0263574726103713 Published online by Cambridge University Press

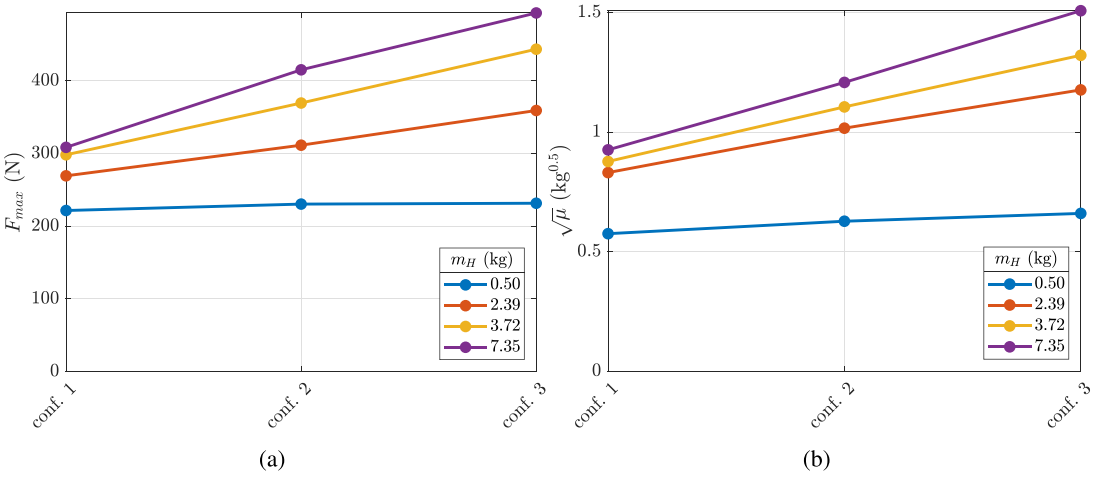


Figure 19. *Peak impact forces (a) and theoretical trend of $\sqrt{\mu}$ (b) for the three robot configurations.*

square root of the reduced mass; therefore, the two trends can be directly compared. A clear qualitative agreement can be observed between the two trends, which validates the theoretical model. In particular, the systematic increase in force with increasing m_H confirms the validity of the theoretical models. Furthermore, the similar slopes of the curves in both graphs demonstrate that the dependence of the impact force on the configuration predicted by the simplified model is confirmed by the experimental results. Minor differences may be attributed to unconsidered experimental factors, such as damping or deformations of the impacting objects, and friction.

Overall, these results demonstrate that despite its simplicity, the proposed lumped-parameter model reliably captures the influence of configuration and obstacle mass on the impact force. Therefore, the lumped parameter model is suitable for fast force estimation and for supporting safety-oriented design and control strategies.

6. Conclusions

In this work, a simplified impact model based on the effective mass concept has been developed. During the impact, the two colliding bodies are modeled as lumped masses. The use of lumped parameters makes it possible a significant reduction in model complexity while preserving consistency with results obtained through more traditional approaches.

The numerical comparison between the simplified model and the full model for a SCARA robot demonstrated their substantial equivalence. The experimental results, carried out through the analysis of planar impacts with a sliding block, confirmed the validity of the proposed model, highlighting its potential as a valuable tool for the design and analysis of robotic systems in collaborative environments.

Future works will include extending the model to robotic manipulators with six and seven degrees of freedom and further investigating safety-related aspects in robotics. In particular, additional experimental tests will be performed to account for factors such as damping or deformations of the impacting objects, friction, and control strategies. Expanding the experimental validation to three-dimensional impacts also represents a promising direction to further enhance the robustness and applicability of the proposed approach.

Author contributions. AC and MB developed the theoretical models and performed the simulations. AC and MT conducted the experimental data collection. AD and GR contributed to the data analysis and interpretation of results and provided methodological support for the simulation models. AC and MB wrote the article. AD, MT, and GR reviewed and revised the article.

https://doi.org/10.1017/S0263574726103713 Published online by Cambridge University Press

Financial support. This research was funded by the European Union – NextGenerationEU – PRIN 2022 – Project. no. 2022XXH9JZ_001/ERC.

Competing interests. The authors declare no conflicts of interest exist.

Ethical approval. Not applicable.

References

[1] S. Robla-Gómez, V. M. Becerra, J. R. Llata, E. Gonzalez-Sarabia, C. Torre-Ferrero and J. Perez-Oria, "Working together: A review on safe human–robot collaboration in industrial environments," *IEEE Access* **5**, 26754–26773 (2017). doi: 10.1109/ACCESS.2017.2773127.

[2] D. Halliday, R. Resnick and J. Walker. *Fundamentals of Physics* (John Wiley & Sons, Hoboken, New Jersey, U.S., 2013).

[3] M. Rodrigues da Silva, F. Marques, M. Tavares da Silva and P. Flores, "A compendium of contact force models inspired by hunt and crossley's cornerstone work," *Mech. Mach. Theory* **167**, 104501 (2022). doi: 10.1016/j.mechmachtheory.2021.104501.

[4] L. Skrinjar, J. Slavič and M. Boltežar, "A review of continuous contact-force models in multibody dynamics," *Int. J. Mech. Sci.* **145**, 171–187 (2018). doi: 10.1016/j.ijmecsci.2018.07.010.

[5] D. Tommasino, M. Bottin, G. Cipriani, A. Doria and G. Rosati, "Development of an End-Effector for Mitigation of Collisions," *International Design Engineering Technical Conferences and Computers and Information in Engineering Conference*, vol. 85437 (American Society of Mechanical Engineers, 2021) p. V007T07A042. doi:10.1115/DETC2021-68928.

[6] ISO 10218-2:2025, Robotics — Safety requirements.

[7] ISO 15066:2016, Robots and robotic devices — Collaborative robots.

[8] M. J. Rosenstrauch and J. Krüger, "Safe Human-Robot-Collaboration-Introduction and Experiment Using ISO/TS 15066," *2017 3rd International Conference on Control, Automation and Robotics (ICCAR)* (IEEE, 2017) pp. 740–744. doi:10.1109/ICCAR.2017.7942795.

[9] J. Falco, J. Marvel and R. Norcross, "Collaborative robotics: Measuring blunt force impacts on humans," *Chest* **140**(210), 45 (2012).

[10] N. G. Dagalakis, J.-M. Yoo and T. Oeste, "Human–robot collaboration dynamic impact testing and calibration instrument for disposable robot safety artifacts," *Ind. Robot Int. J.* **43**(3), 328–337 (2016). doi: 10.1108/IR-06-2015-0125.

[11] A.-C. Huang, K.-J. Lee and W.-L. Du, "Contact force cancelation in robot impedance control by target impedance modification," *Robotica* **41**(6), 1733–1748 (2023). doi: 10.1017/S0263574723000103.

[12] O. Khatib, "Inertial properties in robotic manipulation: An object-level framework," *Int. J. Robot. Res.* **14**(1), 19–36 (1995). doi: 10.1177/027836499501400103.

[13] S.-D. Lee, B.-S. Kim and J.-B. Song, "Human–robot collision model with effective mass and manipulability for design of a spatial manipulator," *Adv. Robot.* **27**(3), 189–198 (2013). doi: 10.1080/01691864.2012.754076.

[14] R. J. Kirschner, N. Mansfeld, G. G. Peña, S. Abdolshah and S. Haddadin, "Notion on the Correct Use of the Robot Effective Mass in the Safety Context and Comments on ISO/TS 15066," *2021 IEEE International Conference on Intelligence and Safety for Robotics (ISR)* (IEEE, 2021) pp. 6–9. doi:10.1109/ISR50024.2021.9419495.

[15] S. Kang, K. Komoriya, K. Yokoi, T. Koutoku, B. Kim and S. Park, "Control of impulsive contact force between mobile manipulator and environment using effective mass and damping controls," *Int. J. Precis. Eng. Manuf.* **11**, 697–704 (2010). doi: 10.1007/s12541-010-0082-4.

[16] A. Caneschi, M. Bottin, A. Doria, A. Cesaro and G. Rosati, "Lumped Parameters Robot Models to Study Impact Dynamics," In: Mechanisms and Machine Science, vol. 165 (2024) pp. 253–260. doi:10.1007/978-3-031-67295-8_28.

[17] A. Cesaro, M. Bottin, M. Tonan, A. Doria and G. Rosati, "Simplified model for dynamic analysis of robotic manipulators," *Int. J. Mech. Control* **26**(1), 119–127 (2025).

[18] O. Khatib, "A unified approach for motion and force control of robot manipulators: The operational space formulation," *IEEE J. Robot. Autom.* **3**(1), 43–53 (1987). doi: 10.1109/JRA.1987.1087068.

[19] B. Siciliano, L. Sciavicco, L. Villani and G. Oriolo, *Robotics Modelling, Planning and Control* (Springer, 2009). doi: 10.1007/978-1-84628-642-1.

[20] M. Tonan, M. Bottin, A. Doria and G. Rosati, "A modal approach for the identification of joint and link compliance of an industrial manipulator," Mechanisms and Machine Science, vol. 122 (2022) pp. 628–636. doi:10.1007/978-3-031-10776-4_72.

[21] G. Antonelli, F. Caccavale and P. Chiacchio, "A systematic procedure for the identification of dynamic parameters of robot manipulators," *Robotica* **17**(4), 427–435 (1999). doi: 10.1017/S026357479900140X.

[22] E. Clochiatti, L. Scalera, P. Boscariol and A. Gasparetto, "Electro-mechanical modeling and identification of the ur5 e-series robot," *Robotica* **42**(7), 2430–2452 (2024). doi: 10.1017/S0263574724000833.

[23] D. Dona', P. Boscariol, M. Bottin, B. Lenzo and G. Rosati, "Static and dynamic identification of the mitsubishi rv-5as-d-s01 robot," *Mech. Mach. Sci.* **163**, 249–256 (2024). doi: 10.1007/978-3-031-64553-2_29.

https://doi.org/10.1017/S0263574726103713 Published online by Cambridge University Press

[24] V. Di Cosmo, A. Giusti, R. Vidoni, M. Riedl and D. T. Matt, "Collaborative Robotics Safety Control Application Using Dynamic Safety Zones Based on the ISO/TS 15066: 2016," *Advances in Service and Industrial Robotics: Proceedings of the 28th International Conference on Robotics in Alpe-Adria-Danube Region (RAAD 2019)* (Springer, 2020) pp. 430–437. doi:10.1007/978-3-030-19648-6_49.

[25] S. B. Hussain, F. Kanwal, "Design of a 3 DoF Robotic Arm," *2016 Sixth International Conference on Innovative Computing Technology (INTECH)* (IEEE, 2016) pp. 145–149. doi:10.1109/INTECH.2016.7845007.

[26] W. C. Jackson and C. PoeJr., "The use of impact force as a scale parameter for the impact response of composite laminates," *Compos. Technol. Res. (ASME)* **15**(4), 282–289 (1993). doi: 10.1520/CTR10380J.

Cite this article: A. Cesaro, M. Tonan, M. Bottin, A. Doria and G. Rosati (2026). "Lumped parameter collision modeling of robotic manipulators based on the effective mass approach", Robotica **44**, 1652–1672. https://doi.org/10.1017/S0263574726103713

https://doi.org/10.1017/S0263574726103713 Published online by Cambridge University Press